Classical Cepheids and RR Lyrae stars: similar, but not too much

G. Bono[1,2], V.F. Braga[1,2,3], A. Pietrinferni[4], D. Magurno[1], M. Dall'Ora[5],

G. Fiorentino[6], K. Fukue[7], L. Inno[8], M. Marengo[9], M. Bergemann[8], R. Buonanno[4],

R. da Silva[3], M. Fabrizio[3], I. Ferraro[2], R. Gilmozzi[10], G. Iannicola[2], W. Kausch[11,12],

N. Kobayashi[7], V. Kovtyukh[13], B. Lemasle[14], M. Marconi[5], S. Marinoni[3],

P.M. Marrese[3], C.E. Martínez-Vázquez[15], N. Matsunaga[7], M. Monelli[15], J. Neeley[9],

M. Nonino[16], B. Proxauf[17], N. Przybilla[12], M. Romaniello[10], M. Salaris[18],

C. Sneden[19], P.B. Stetson[20], F. Thévenin[21], T. Tsujimoto[22], M. Urbaneja[12],

E. Valenti[10], and M. Zoccali[23,24]

(Affiliations can be found after the references)

Abstract. We discuss evolutionary and pulsation properties of classical Cepheids and RR Lyrae stars. We focus our attention on the role that they play as standard candles and as tracers of young and old stellar populations. We also introduce some plain physical argument concerning the occurrence of optical/near-infrared Period-Luminosity relations in classical Cepheids and in RR Lyrae. Moreover, we outline pros and cons of the different diagnostics adopted to estimate individual distances, and in particular, the uncertainties affecting reddening and chemical compositions. We also address some relevant issues concerning optical and Near-Infrared (NIR) spectroscopy of radial variables. Finally, we briefly outline near future experiments concerning Galactic and extra-galactic stellar variability projects.

1. Introduction

Classical Cepheids (CCs) and RR Lyrae stars (RRLs) are becoming more and more popular, this revival applies not only to astrophysical, but also to cosmological open problems. This new interest in radial variables that are very accurate distance indicators and solid stellar tracers started with the release of the first optical catalogs of microlensing experiments in the Galactic Bulge (Udalski et al.

1993) and in the Magellanic Clouds (MCs Udalski et al. 1998). A significant step forward in this direction is the recent release of the new catalogs by OGLE IV (Soszyński et al. 2014; Pietrucowicz et al. 2015), including more than 9500 Cepheids and 45000 RRL in the Magellanic Clouds and more than 38000 RRL in the Galactic Bulge.

The quoted long-term variability surveys towards specific targets have been soundly complemented by more recent optical surveys

covering a significant fraction of the Galactic Halo (Catalina, Drake et al. 2014; Torrealba et al. 2015; ASAS, Pojmanski et al. 2005; PTF, Rau et al. 2009; SDSS, Gunn et al. 1998) and of the thin disk (KISOGP, Matsunaga et al. 2016b).

The new near-infrared wide field detectors opened also the path to new NIR surveys toward the Galactic center (IRSF@SIRIUS, Matsunaga et al. 2016a), the bulge and the Galactic thin disk (VVV@VISTA, Minniti et al. 2010) and the Magellanic Clouds (IRSF@SIRIUS, VMC@VISTA, Inno et al. 2015; Cioni et al. 2011).

The spectroscopic investigations focussed on RRLs and CCs lag when compared with the photometric ones. The reasons are manifold. The density of RRLs in the Galactic halo is roughly one per square degree, but the current fiber and slit multi-object spectrographs have FoV that are smaller than one square degree (VIMOS and FLAMES at VLT, Le Fèvre et al. 2003; Pasquini et al. 2002; GMOS at Gemini, Hook et al. 2004; DEIMOS and MOSFIRE at Keck, Faber et al. 2003; McLean et al. 2012; M2FS at Magellan, Mateo et al. 2012). The only exception is the 2DF at the AAT offering up to 392 fibers and a field of view of 2 square degrees (ARGOS, Ness et al. 2012; BRAVA, Kunder et al. 2012; RAVE, Steinmetz et al. 2006). The same outcome applies to APOGEE (300 fibers and a FoV of 2 square degrees, Majewski et al. 2015) observing in high resolution in the H band and to LAMOST for optical low-resolution spectra.

The density of RRLs in the Galactic bulge, in particular approaching the inner bulge is higher (see Fig. 3 in Pietrucowicz et al. 2015) and they become more suitable for MOS observations (Zoccali et al. 2004). The spatial distribution of the currently known CCs (∼550) is also too sparse to justify a MOS to investigate their kinematics and chemical abundances. The new generation of wide field multi-object spectrographs are going to have a larger field of view such as 4MOST (4 square degrees and 2400 fibers, de Jong et al. 2014), MSE (1.5 square degrees and 3200 fibers, McConnachie et al. 2016) and WEAVE (3 square degrees, ∼ 1000 fibers, Dalton et al. 2014).

The above limitations explain the limited, if any, massive spectroscopic investigations focussed on RRL and CCs.

On top of these observational limitations, the RRLs have also been poorly investigated from the spectroscopic point of view because in the atmosphere of fundamental pulsators, along the rising branch, form and propagate strong shocks causing severe nonlinearities in the formation of both strong and weak lines. To overcome these problems there are two possible paths: either to collect the spectra at fixed pulsation phase or to collect the spectra with 8m class telescopes requiring short exposure time. In dealing with Time Allocation Committees both of them are not trivial issues.

The structure of the paper is the following: in §2 and 3 we discuss the most relevant empirical evidence concerning the classification and the main pulsation properties of CCs and RRLs respectively. The key evolutionary features and the plane physical arguments driving the occurrence of the Period-Luminosity (PL), Period-Luminosity-Color (PLC) and Period-Wesenheit (PW) relations are outlined in §4 and 5. The impact that the reddening law has on different wavelength regimes is discussed in §6, while in §7 we outline the future perspectives for radial variables in the Gaia era. The current status concerning high-resolution spectroscopic surveys focussed on CCS and on RRLs are discussed in §8 together with a few relevant issues concerning optical and NIR spectroscopic diagnostic. The future perspectives of the current project and the impact that ground-based and space facilities with have on cosmic distances and stellar tracers are outlined in §9.

2. Classical Cepheids pulsation properties

CCs, according to their pulsation properties can be split into four sub-groups:

1) Fundamental – Variables that pulsate in the fundamental mode. The theoreticians call them either "F" or "FU" pulsators, while the observers call them DCEPs. Their luminosity amplitudes range from 1.5 to a few tenths of magnitude, while the radial velocity (RV) am-
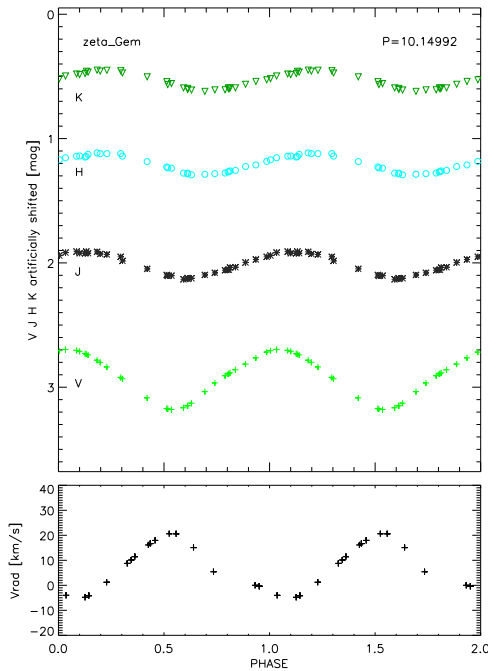
Fig. 1. Top: Optical/near-infrared (*VJHK*(light curves of the Galactic CC ζ Gem (fundamental). The light curves were arbitrarily shifted to avoid overlap, the photometric bands are labelled on the left side. The pulsation period (days) is labelled in the top right corner. Time series were collected by Laney & Stobie (1992). Bottom: Radial velocity curve based on homogeneous high-resolution spectra (Proxauf et al. 2016).

plitudes are of the order of 20-40 km/sec (bottom panel of Fig. 1). The amplitude distribution in the Bailey diagram is similar to a "V shape" and the minimum takes place at the center of the so-called Hertzsprung progression (HP). Nonlinear phenomena do occur in CCs, but their formation and propagation is typically sub-sonic (Sasselov & Lester 1994; Nardetto et al. 2008).

2) First Overtone – Variables that pulsate in the first overtone mode. The acronym adopted by observers is "SCEP", while theoreticians call them "FOs". Their luminosity and RV amplitudes are on average a factor of two smaller than for FU ones and the shape of their light curve is more sinusoidal. Their period distribu-

tion is narrower when compared with the fundamental one and the long-period tail is metal dependent, indeed it becomes longer when moving towards more metal-poor stellar systems (Bono et al. 2005).

3) Second Overtone – Variables that pulsate in the second overtone mode. The theoreticians call them "SO" pulsators. Their luminosity amplitude are of the order of a few tenths of a magnitudes and their amplitudes are smaller than for FU and FO ones.

Overtone pulsators share common features: a) higher overtones are, at fixed pulsation period, brighter than fundamental ones; b) the region of the instability strip in which they are pulsationally stable are systematically hotter (bluer) when moving from fundamentals to overtones.

4) Mixed–Mode Variables that pulsate simultaneously either in one overtone (first, second) plus the fundamental mode or in two overtones. The theoreticians call them "Beat" Cepheids (Cox 1980).

On top of the above modal classifications, fundamental Cepheids also display the Hertzsprung Progression. In the period range between ~6 and ~10 days Galactic Cepheids show a well defined bump along the light and the radial velocity curves. The theoreticians call them "Bump" Cepheids (Cox 1980). The phase at which the bump shows up depends on the pulsation period. It is located on the rising branch in the short-period range (P = 6–8 days), approaches the phases of maximum light at the center of the HP (P = 8–8.5 days) and moves along the decreasing branch in the long-period range (P = 8.5–10 days). Note that Cepheids located at the center of the HP attain very small amplitudes. Moreover, it is worth mentioning that the period range and the center of the HP does depend on the metal content, and indeed there is evidence that a decrease in metal content causes a steady increase in the period of the HP center. Empirical evidence based on large sample of Magellanic Cepheids indicate that the center of the HP in the Large Magellanic Cloud (LMC) is at P=11.24 days, while in the Small Magellanic Cloud (SMC) is at P=11.00 days (Bono, Marconi, & Stellingwerf 2000).

The appearance of a bump that changes as a function of the pulsation period has also been suggested for the first overtones (Moskalik et al. 1992) and for the long-period Cepheids (Buchler 2009).

The reason why we do not have specific empirical names for CCs pulsating in different modes is because, till the early nineties, it was not clear whether they could also pulsate in the first overtone (Bohm-Vitense 1988). The microlensing experiments targeting the Magellanic Clouds (MACHO, Alcock et al. 2000; EROS, Marquette et al. 2009; OGLE, Udalski et al. 2015) demonstrated, on the basis of the period-luminosity plane, that they pulsate in the fundamental, in the first overtone and in the second overtone. Moreover, they also discovered a large variety of mixed–mode variables, while only a few of them were previously known in the Milky Way (Poretti, Baglin, & Weiss 2014).

3. RR Lyrae pulsation properties

The RRLs according to their pulsation properties can be split into three sub-groups:

1) RRab – Variables that pulsate in the fundamental mode. The observers call them RRab, while the theoreticians do prefer to call them either "F" or "FU" pulsators. Their luminosity amplitudes in the V band range from a few tenths to 1.5 magnitudes, while the radial velocity (RV) amplitudes are of the order of 40-70 km/sec (bottom panel of Fig. 2). Both RV and light variations draw a saw-tooth curve along the pulsation cycle. The Bailey diagram (luminosity amplitude versus period) clearly shows how their amplitudes steadily decrease when moving from the blue to the red edge of the F instability region (Stetson et al. 2014; Fiorentino et al. 2015).

2) RRc – Variables that pulsate in the first overtone mode. The theoreticians call them "FO" pulsators, while the observers RRc. Their luminosity and RV amplitudes are on average a factor of two smaller than for RRab. Moreover, light and RV variations are smooth over the entire cycle (Fig. 3). The amplitude distribution in the Bailey diagram is approximated by a parabola and is commonly called
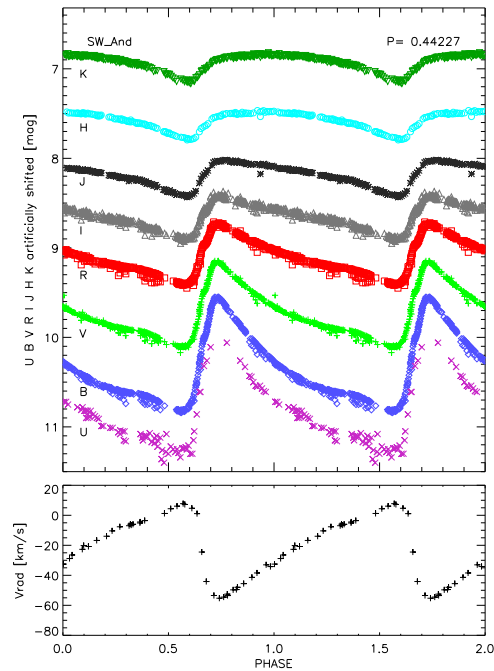

Fig. 2. Top: Optical/near-infrared (*UBVRIJHK*) light curves of the Galactic field RR Lyrae SW And. This variable pulsate in the fundamental (RRab) and its period is labelled in the top right corner (in days). The light curves were arbitrarily shifted to avoid overlap, the photometric bands are labelled on the left side. Time series were collected by Cacciari et al. (1987); Barnes et al. (1988); Liu & Janes (1989); Jones et al. (1992). Note the steady decrease in luminosity amplitude when moving from bluer to redder photometric bands. Bottom: Radial velocity curve provided by (Liu & Janes 1989).

either a "bell" (Bono et al. 1997a) or a "hairpin" (Kunder et al. 2013) distribution.

3) RRd – Variables that pulsate simultaneously in the first overtone (main) and in the fundamental (secondary) mode. The observers call this group RRd, while the theoreticians do prefer to call them either "double–mode" or "mixed–mode" pulsators. The former definition was originally adopted, since only two frequencies were typically detected. However, the unprecedented time series data collected from space (CoRoT, Poretti et al. 2010; Chadid et al. 2011; Kepler, Molnar 2016) revealed a com-
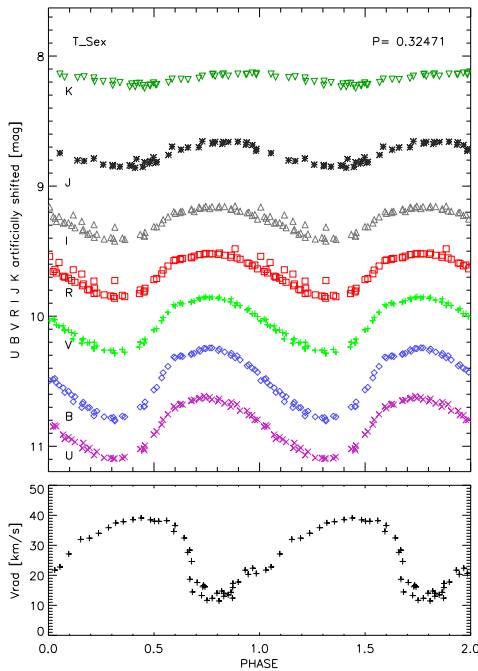
Fig. 3. Top: Same as Fig. 2, but for the first overtone (RRc) Galactic field RR Lyrae T Sex. Time series collected by Barnes et al. (1988); Liu & Janes (1989); Jones et al. (1992). Note the sinusoidal shape of the light curves. Bottom: Radial velocity curve provided by (Liu & Janes 1989)
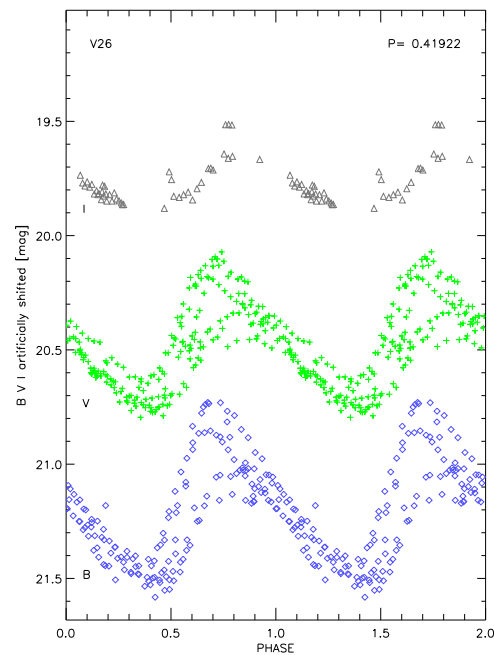
Fig. 4. Optical (*BVI*) light curves of the mixed–mode RR Lyrae (RRd) V89 in the Carina dSph (Coppola et al. 2015). The period of the main pulsation mode (first overtone) is labelled in the top right corner. Note the significant modulation in phase and in luminosity amplitude.

plex frequency spectrum. The variations affect the light and RV curves over the entire pulsation cycle by a few tenths of optical magnitudes (Fig. 4) and a few tens of km/sec.

From time to time it has also been suggested the possible occurrence of RRLs pulsating in the second overtone mode (Clement & Rowe 2000) at very short periods. The observers call them RRe, while the theoreticians call them "SO". However, solid theoretical predictions indicate that SOs do not attain a stable limit cycle (Bono et al. 1997b). At the same time, theory indicates that more metal-rich HB stars can produce short period FOs, i.e. RRLs covering the short period tail of FOs (Bono et al. 2001; Dall'Ora et al. 2003).

Fundamental RRLs are also affected by the so-called Blazhko effect, i.e. a secondary modulation of both amplitude and pulsation phase.

Recent estimates indicate that at least one third of RRab and a minor fraction of RRc variables show a secondary modulation ranging from a few tens of days to years during which the amplitude and its phase change as a function of time. The modulation is of a few tenths of magnitude and of a few tens of km/sec for the light and radial velocity curves respectively (Fig. 5). Empirical evidence indicates that this phenomenon only takes place in RRLs with periods shorter than ~0.65 days (Braga et al. 2016). This means that convection plays a crucial role in quenching the physical mechanism(s) driving the occurrence of this phenomenon. The convective timescale and the thickness of the convective envelope steadily increases when moving from the blue (hot, shorter periods) to the red (cool, longer periods) edge of the instability strip (Bono & Stellingwerf 1994;
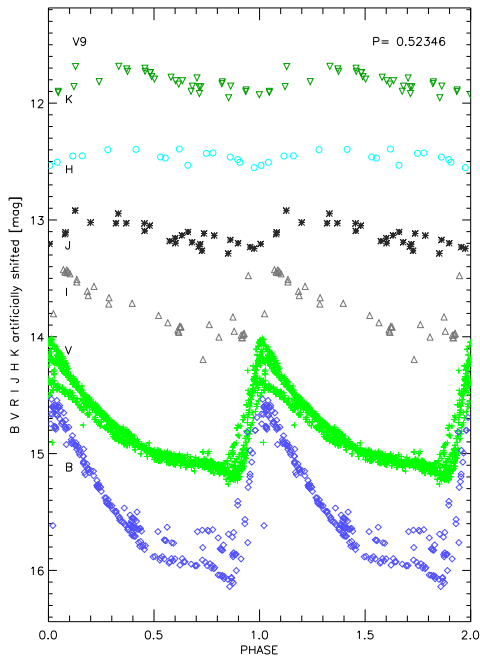
Fig. 5. Optical/near-infrared (*BVIJHK*) light curves of the candidate Blazhko variable V9 in the Galactic globular ω Cen (Braga et al. 2016). This variable pulsate in the fundamental mode and its period is labelled in the top right corner. Note the steady decrease in amplitude modulation when moving from optical to NIR bands.

Bono et al. 1997a). However, we still lack a detailed physical understanding of the physical processes causing the occurrence of this phenomenon and its dependence on input parameters (Stothers 2006; Chadid et al. 2011). Note that time series collected with space telescopes have also disclosed the occurrence of a third longer modulation (Bryant 2014), but the current data do not allow us to constrain the periodicity of this component.

During the last few years there is mounting empirical evidence that a fraction of RRc variables are also affected by the Blazhko phenomenon (from 5% to >50%, Kunder et al. 2013).

4. Classical Cepheid as standard candles

One of the fundamental ingredients in dealing with the PL relations of CCs is the Mass–Luminosity (ML) relation of intermediate–mass stars. This is a longstanding astrophysical problem, since the size of the He core after central Hydrogen burning phases, and in turn, the ML relation depends on different physical mechanisms structures (Chiosi & Maeder 1986; Brocato & Castellani 1993; Stothers & Chin 1993, 1994; Cassisi & Salaris 2011; Bono et al. 2010; Prada-Moroni et al. 2012; Anderson et al. 2016).

Among them the most relevant are:

i) Extra-mixing – i.e., an increase in the efficiency of convective core over-shooting during central Hydrogen burning phases increases the He-core size;

ii) Rotation – i.e. the sheer of the layers located at the interface between convective and radiative regions causes a larger internal mixing, and in turn, a larger He-core size;

iii) Radiative opacity – i.e. an increase in stellar opacity causes an increase in the central temperatures, and in turn in the efficiency of central Hydrogen burning and in the efficiency of the convective transport, and therefore an increase in the He-core size;

iv) Mass Loss – efficiency of mass loss along the Main Sequence, the Hayashi track, and the blue loop. An increased efficiency in mass loss causes a decrease in the envelope mass, and in turn, an increase in the luminosity at fixed mass.

In the following we briefly discuss the impact that extra–mixing and rotation have on the ML relation. From top to bottom Fig. 6 shows theoretical predictions according to Pietrinferni et al. (2004), for three different chemical compositions representative of SMC (Z=0.004), LMC (Z=0.08) and Milky Way (Z=0.0198) Cepheids. Note that the stellar structures located inside the instability strip were selected following the same approach adopted by Bono et al. (2010). In particular, the adopted stellar isochrones are based on detailed sets of evolutionary models computed assuming a scaled solar chemical compositions
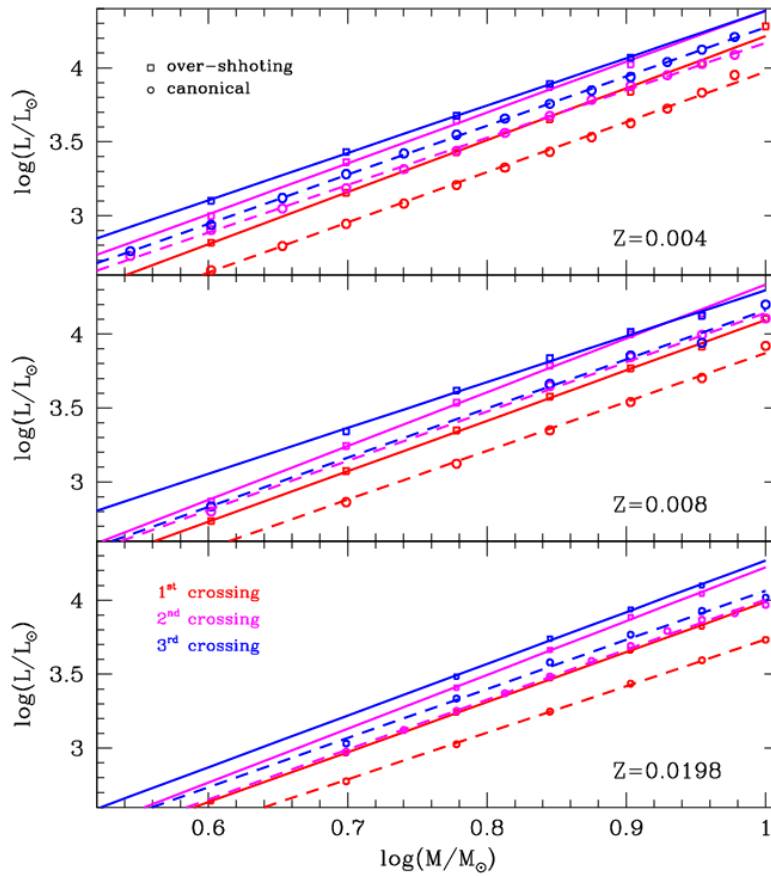
Fig. 6. Top: Predicted Mass–Luminosity (ML) relation for intermediate-mass stars, for a chemical composition representative of SMC Cepheids (Z=0.004, Y=0.251) and for the first (red), second (purple) and the third (blue) crossing of the instability strip. Stellar isochrones based on evolutionary models that either neglect (canonical) or take account of convective core over-shooting during central Hydrogen burning phases (non-canonical) are marked with circles and squares, respectively. Middle: Same as the top, but for a metal content representative of LMC Cepheids (Z=0.008, Y=0.256). Bottom: Same as the top, but for a metal content representative of Galactic Cepheids (Z=0.02, Y=0.2734).

and the solar mixture provided by Grevesse & Noels (1993). To quantify the difference among the multiple crossings of the Cepheid instability strip we took account of the first (red), the second (magenta) and the third (blue) crossing. Moreover, to evaluate the impact that the efficiency of over-shooting during central hydrogen burning phases has on the size of the convective core, we took account for both canonical (no overshooting, circles) and non-canonical (mild overshooting, squares) evolutionary models. To perform a more quantitative analysis of the difference among the quoted evolutionary phases, we also computed linear regressions of the form

$$\log(L/L_\odot) = \alpha + \beta\log(M/M_\odot) + \gamma[Fe/H]$$

where the symbols have their usual meaning. The coefficient of the ML relations for canoni-
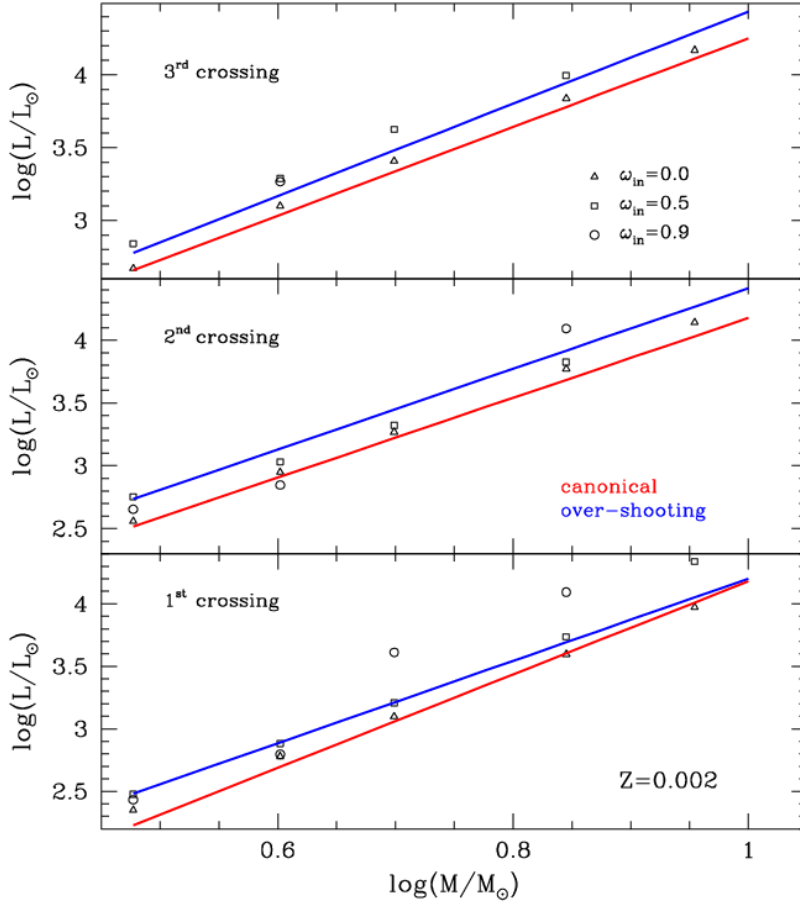
Fig. 7. Top: Comparison among predicted ML relations for a metal-poor scaled solar chemical composition (Z=0.002, Y=0.248) and for the third crossing of the instability strip. The solid lines display the ML relations for evolutionary models constructed either neglecting (red) or taking into account (blue) convective core over-shooting during central hydrogen burning phases. The black symbols display ML values for evolutionary models constructed either neglecting rotation (triangles) or assuming mild rotation (squares) or strong rotation (circles). Middle: Same as the top, but for the second crossing. Bottom: Same as the top, but for the first crossing.

cal and non-canonical evolutionary models and for the three different crossings and chemical compositions are listed in Table 1. Note that empirical and theoretical evidence clearly indicate that the first crossing is significantly faster than the subsequent crossings (Bono et al. 2010; Anderson et al. 2016). This is the reason why we also estimated a global ML relation taking account of both canonical and non-canonical models and both 2nd and 3rd crossings. The coefficient of this global ML relation are also listed in Table 1.

The predictions plotted in this figure display the expected trends. The luminosity of the different crossings, at fixed stellar mass, steadily increases when moving from the first

to the third crossing. Note that the difference is far from being constant when moving from lower to higher masses. This is the consequence of two well known problems in dealing with the advanced evolutionary phases of intermediate-mass stars. In particular, the extent in effective temperature, and the shape of the blue loops do depend on the treatment of different physical mechanisms (mass loss, overshooting [core and envelope], treatment of the convective transport, rotation) and on the input physics (opacities, nuclear reactions, helium-to-metals enrichment ratios, mixing length parameters) (Bono et al. 2010; Prada-Moroni et al. 2012; Anderson et al. 2016).

Non-canonical models are, at fixed stellar mass and chemical composition, on average 0.15 dex brighter than the canonical ones. The difference is not constant across the mass range covered by the current models. Moreover, the difference shows a mild increase when moving from metal–poor to metal–rich stellar structures.

To further constrain the difference of the current theoretical framework with the evolutionary and pulsation prescriptions recently provided by Anderson et al. (2016), Fig. 7 shows the comparison for Z-0.002. Note that we adopted the Grevesse & Noels (1993) solar mixture, while Anderson et al. (2016) adopted the Asplund et al. (2009) chemical mixture and their solar metallicity is Z=0.014. However, the comparison is only minimally affected by the difference in the adopted solar mixture. Predictions plotted in this figure indicate that the three crossings of the current canonical models agree quite well with Anderson's models neglecting rotation (triangles). The same agreement applies to the current non–canonical models and the Anderson's models with mild–rotation (squares, ω_{in}=0.5), and indeed the difference in luminosity is on average smaller than 0.1 dex. On the other hand, the Anderson's models with strong rotation (open circles, ω_{in}=0.9), are at least 0.1 dex brighter than current evolutionary prescriptions.

The above findings indicate that the difference in luminosity can be barely adopted to discriminate among the different evolutionary frameworks. The difference in the relative abundances of CNO elements appear to be the acid test to constrain the efficiency of the physical mechanisms driving the size of the helium core of intermediate-mass stars (Castellani et al. 1990; Prada-Moroni et al. 2012; Anderson et al. 2014).

To further constrain the impact that the ML relation has on the PL relation of CCs, Fig. 8 shows the correlation between the luminosity (top), the visual magnitude (middle) and the K-band magnitude with the stellar mass. We selected the CCs along the second crossing and for two different chemical compositions (see labelled values). Evolutionary prescriptions plotted in this figure display several interesting features: a) Relatively metal-poor Cepheids cover ~1.5 dex in luminosity when moving from low- to high-mass Cepheids, this means more than three V-band magnitudes and four K-band magnitudes. c) Relatively metal-poor, intermediate-mass stellar structures naturally produce short period Cepheids when compared with more metal-rich structures, since their blue loops are, at fixed stellar mass, more extended in effective temperature (Bono et al. 2010; Prada-Moroni et al. 2012). The period distribution of the metal–poor models plotted in Fig. 8 ranges from ~1 to ~45 days, while for the more metal–rich it ranges from a few days to more than ~60 days. b) The K-band magnitudes, in contrast with the visual magnitudes, are less sensitive to the metal content, in particular, in the high–mass regime.

The use of CCs as standard candles has been addressed in many recent investigations. During the last few years the attention was focussed on the impact that optical, NIR and Mid-Infrared (MIR) photometry has on the zero-point (Riess et al. 2016) and on the slope (Inno et al. 2016) of the diagnostics adopted to estimates their distances. Pros and cons of Population I and Population II standard candles were discussed on quantitative bases by Beaton et al. (2016). A significant step forward in the discussion of accuracy of CCs as standard candles has been made by the use of NIR (Welch et al. 1987; Persson et al. 2004) and MIR (Marengo et al. 2010; Ngeow & Kanbur
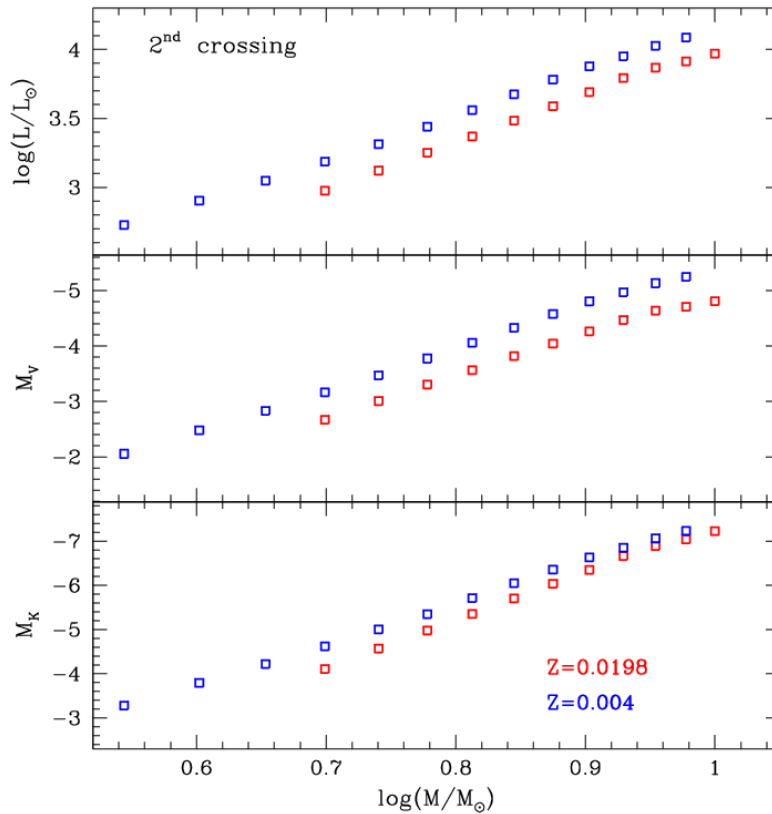
Fig. 8. Top – Predicted Mass–Luminosity relation for canonical Classical Cepheids along the second crossing of the instability strip. Blue and red symbols display different masses at Z=0.004 typical of SMC Cepheids and at Z=0.0198 typical of Galactic Cepheids. The labels display the period range when moving from short– to long–period Cepheids. Middle – Same as the top, but for the predicted visual magnitudes. Bottom – Same as the top, but for the predicted K-band magnitudes.

2010; Freedman et al. 2012) mean magnitudes. This provides the unique opportunity to provide a large set of distance diagnostics base on optical/NIR/MIR magnitudes. In dealing with these new datasets we have to take account of two competing factors.

a) Color index - Larger is the difference between the central wavelength of the bands adopted to compute the colors, smaller are the color coefficients in the Wesenheit index (Inno et al. 2015; Braga et al. 2015). This means that optical-NIR and optical-MIR colors are

less prone to photometric uncertainties affecting the mean colors.

b) Photometric accuracy - The current photometric surveys are mainly performed in optical bands. This means that the optical mean magnitudes are more accurate than the NIR/MIR ones. In these regimes, we typically have only a few random measurements but the precision on the mean magnitudes can be improved by using template light curve when available (Inno et al. 2015). The lack of accurate template light curves and/or accurate pulsation parameters (epoch of mean/maximum
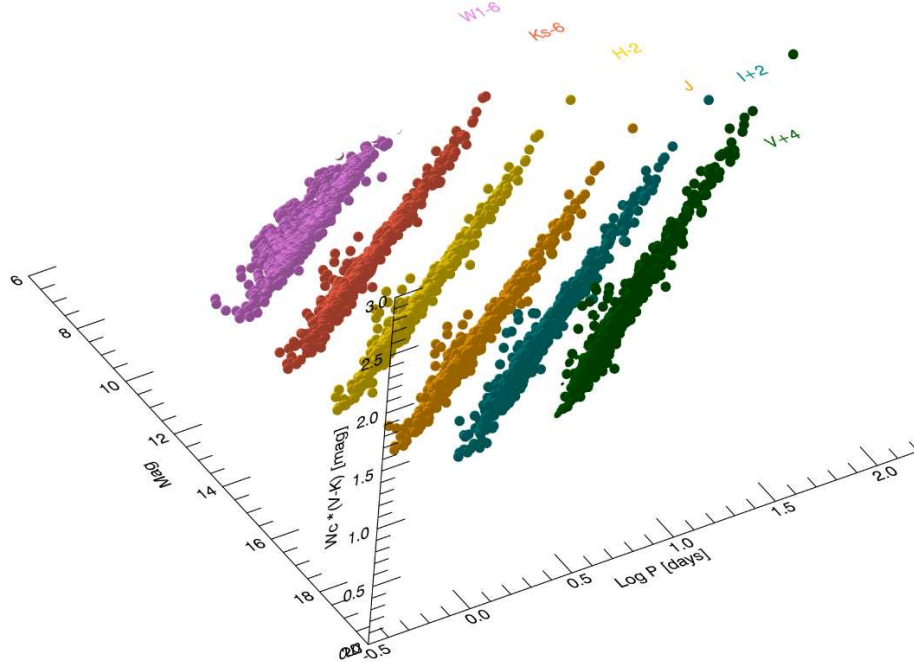
Fig. 9. Optical, NIR and MIR three dimensional Period-Wesenheit relations for LMC classical Cepheids (Inno et al. 2016). Note that the current data were plotted using the same color index (V K) for all the PW relations. We adopted the following Wesenheit coefficients (Cardelli et al. 1989): $A_V/(A_V-A_Ks)$= 1.14, $A_I/(A_V-A_Ks)$= 0.69, $A_J/(A_V-A_Ks)$= 0.33, $A_H/(A_V-A_Ks)$= 0.21, $A_Ks/(A_V-A_Ks)$= 0.14, $A_w1/(A_V-A_Ks)$= 0.06. The different PW relations were artificially shifted in magnitude to avoid the overlap. Note that the current data were plotted using the same color index $(V - K)$ for all the PW relations.

light, optical amplitudes) implies that instantaneous measurements are affected by the photometric error plus an error given by the semi-amplitude of the adopted NIR/MIR band.

The impact of the quoted issues are displayed in Fig. 9 for LMC CCs. Optical (*V*,*I*) mean magnitudes plotted in this figure come from well sampled light curves collected by OGLE IV (Soszyński et al. 2015), while NIR (*JHK*) mean magnitudes come from different sources ranging from well sampled light curves to either a few or to individual measurements (Inno et al. 2016). The MIR data are based on time series collected in the w1 band by WISE

(Cutri & et al. 2013). The different data sets plotted in this figure were already corrected for depth effects across the body of LMC. This means that the spread on the individual relations, and in turn the precision on the individual distances, is mainly driven by photometric uncertainties either in the NIR or in the MIR bands.

5. RR Lyrae as standard candles

The RRLs have been considered robust standard candles because they obey to a well defined M_V vs iron abundance relation (Sandage
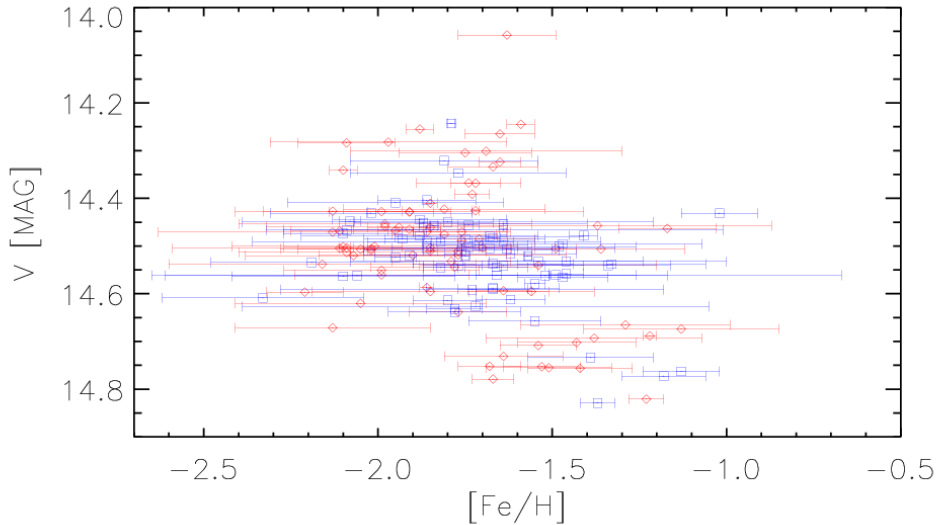
Fig. 10. Top – Position in the *V*-[Fe/H] plane of the fundamental (red) and first overtone (blue) RR Lyrae in the GGC ω Cen. The iron abundances are the means between the spectroscopic estimates provided by Sollima et al. (2006) and the photometric metallicities provided by Rey et al. (2000). The horizontal bars display the error on the mean metallicities.

1990; Caputo 1998). However, this diagnostic is affected by several possible systematics.

a) Reddening – This diagnostic is prone to uncertainties in reddening correction, and indeed an error of 3% in reddening means an error of the order of 10% in distance modulus. This problem becomes even more severe in dealing with stellar systems affected by differential reddening (Braga et al. 2015).

b) Linearity – There are empirical and theoretical arguments to believe that this diagnostic is not linear over the entire metallicity range (more than three dex) covered by field and cluster RRLs (see Caputo et al. 2000; Rey et al. 2000; Bono et al. 2003). This effect mainly affects the metal–poor (Halo) and the metal–rich (Bulge) tail of field RR Lyrae stars. This issue is further complicated by the trend of α-elements when moving from the metal-poor (typically enhanced) to the metal-rich (either slightly enhanced or solar) regime (see figures 6 and 7 in McWilliam 2016).

c) Evolutionary effects – the current photometric data do no allow us to quantify the off Zero-Age-Horizontal-Branch (ZAHB) evolution of individual RR Lyrae stars. This is a thorny effect, since the range in luminosity in which the RRLs spend a significant fraction of the their lives increases when moving from metal–poor ($Z=0.0001$, $\Delta V \approx 0.7$ mag) to metal–rich ($Z=0.01$, $\Delta V \approx 1.0$ mag) stellar structures.

d) Metallicity – The use of individual metallicities and their uncertainties strongly limit the application of this diagnostic. Data plotted in Fig. 10, show the impact that a spread in iron abundance (Braga et al. 2016), differential reddening (Calamida et al. 2005) and evolutionary effects (Castellani et al. 2007) have on RRLs of the Galactic globular ω Cen.

Dating back to the seminal investigation by (Longmore et al. 1986) it became clear that the NIR PL relations have different key advantages in estimating individual RRL distances. Indeed, the impact of reddening uncertainties is on average a factor of two smaller (Cardelli et al. 1989). Moreover and even more important, the PL relations are linear and the spread

both in the NIR (Braga et al. 2015; Marconi et al. 2015) and in MIR (Neeley et al. 2015) PL relations is of the order of a few hundreds of magnitude.

The quoted advantages become even more relevant for stellar systems affected by differential reddening. Data plotted in Fig. 11 display the variation in the intrinsic dispersion of the PL relation for RRLs in the Galactic globular M4, when moving from the I-band (top) to the J-band (middle) and to the K-band (bottom). A detailed spectroscopic investigation based on large sample of high resolution spectra of cluster stars (RG+SG+MS) indicates a minimal variation in iron abundance ([Fe/H]=-1.16±0.09/-1.07±0.02, Malavolta et al. 2014). The reddening variation in this cluster was recently investigated by Hendricks et al. (2012). They found a mean reddening E($B − V$)=0.37 mag and a reddening variation across the body of the cluster of ±0.10 mag. The photometric accuracy of the IJK mean magnitudes of RRLs is quite similar (Stetson et al. 2014). The intrinsic dispersion (see vertical bars) due to the reduced impact of the differential reddening decreases from 0.07 mag in the I-band, to 0.06 mag in the J-band and to 0.04 mag in the K-band.

In spite of the quoted indisputable advantages of NIR and MIR PL relations, these diagnostics are still prone to two sources of systematic errors: a) individual reddening corrections; b) individual metal abundances in the slope and/or in the zero-point (Bono et al. 2003; Marconi et al. 2015). The top panel of Fig. 12 shows these effects using the I-band PL relation. There is a significant improvement when moving from the M_V vs [Fe/H] relation to the I-band PL relation, but the spread around the relation is still dominated by uncertainties on individual metallicities.

It came as a surprise the theoretical (Marconi et al. 2015) and the empirical (Martínez-Vázquez et al. 2015; Braga et al. 2016) evidence that optical Period-Wesenheit relations are only marginally affected by metal content. This means that the metallicity dependence of the V-band is almost perfectly counterbalanced either by the $B − V$ or by the $B − I$ color. Indeed the metallicity coef-

ficient in the quoted PW relations is smaller than 0.1 dex/mag. Data plotted in the bottom panel of Fig. 12, display the $V,B − I$ PW relation and the intrinsic dispersion for fundamental and first overtone pulsators is identical to the dispersion of the I-band PL relations. The Wesenheit index is also a pseudo-magnitude that is reddening-free by construction (Madore 1982; Inno et al. 2015; Braga et al. 2015). This positive feature relies on the assumption that the reddening law we adopt to estimate the selective absorption coefficients is universal (Inno et al. 2016).

The optical (VBI) PW relations when applied to RRLs offer the double key advantages to be minimally affected by metallicity and by uncertainties in reddening corrections.

To further quantify the physical mechanisms driving the occurrence of the PL relation in RRLs and in CCs, the top panel of Fig. 13 shows the ML relation for low-mass central helium burning stellar structures along the ZAHB phase. Lines of different colors display evolutionary prescriptions for metal-poor (Z=0.0003), metal-intermediate (Z=0.001) and relatively metal-rich (Z=0.008) stellar structures. The three different sets of models display two well-known trends: a) an increase in the metal content causes a systematic decrease in the mean mass population of the RRL instability strip (squares), and in turn in its mean luminosity; b) an increase in the metal content causes a systematic decrease in the range of stellar masses populating the RRL instability strip. The spread in mass for the metal-poor composition is ∼0.055 $M_\odot$, while in the metal-rich one is ∼0.011 $M_\odot$. On the other hand, the difference in luminosity is ∼0.045 and ∼0.035 dex, respectively.

However, the above difference in stellar mass and in luminosity causes a marginal difference in visual magnitude. A glance at the predictions plotted in the middle panel display quite clearly that visual magnitude is almost constant at fixed chemical composition. This supports the lack of a well defined V-band PL relation. On the other hand, predictions for the K-band plotted in the bottom panel of the same figure display a change of at least half a magnitude when moving from the blue to the red
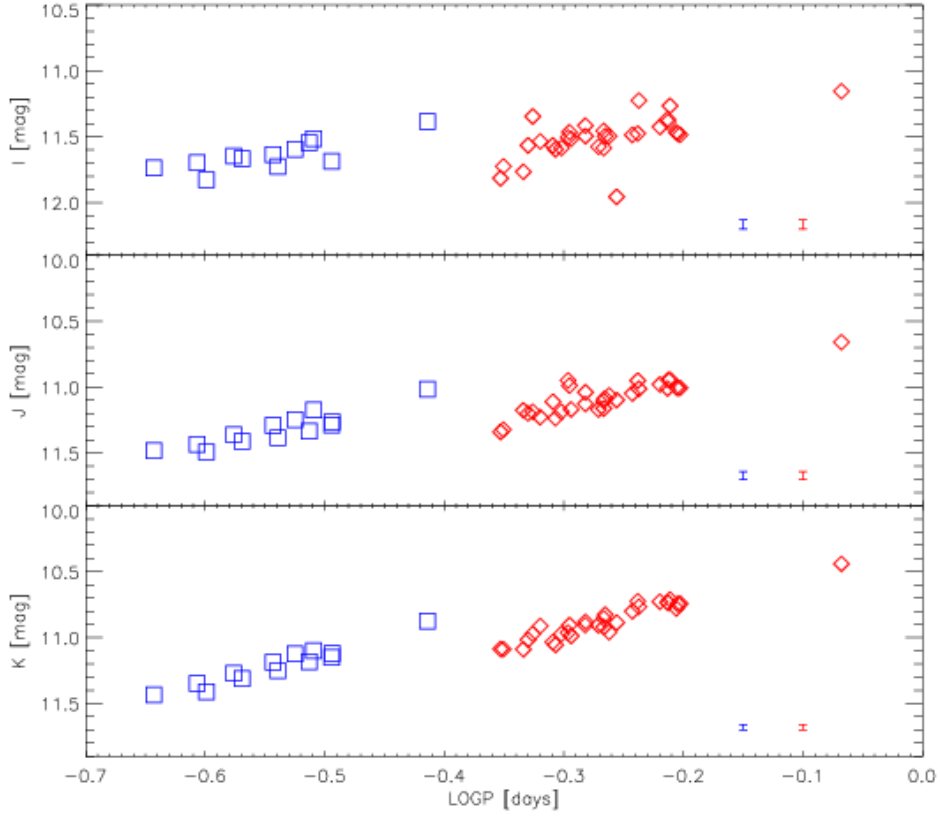
Fig. 11. Top – *I*-band Period-Luminosity relations for fundamental (red) and first overtone (blue) RR Lyrae of the GGC M4 (Stetson et al. 2014; Braga et al. 2015). The vertical bars plotted in the right bottom corner display the standard deviations of the PL relations. Middle – Same as the top, but the *J*-band PL relation. Bottom – Same as the top, but the *K*-band PL relation.

edge of the instability strip. This evidence becomes even more compelling if we take account for the change in pulsation period between the blue to the red edges of the instability strip. The pulsation periods listed in column 5 of Table 2 indicate that this difference is of the order of 0.4 days.

The above plain physical arguments indicate that RRLs display a PL relation in the NIR bands due to significant change in bolometric corrections as originally suggested by Bono et al. (2003). This is a substantial difference when compared with CCs in which the PL shows up in all the photometric bands, due to the significant change in ML relation when moving from lower to higher stellar masses.

In passing we note that the above arguments concerning the RRL PL relation relies on a crude approximation, i.e. we are assuming that all the stellar structures spend a significant fraction of their lifetime on the ZAHB. More detailed calculations based on synthetic HB models properly accounting for off-ZAHB evolution are required to quantify the impact on pulsation period of the change in surface gravity and in effective temperature.

6. Reddening laws

Recent determination of the interstellar extinction curve (Rieke & Lebofsky 1985;
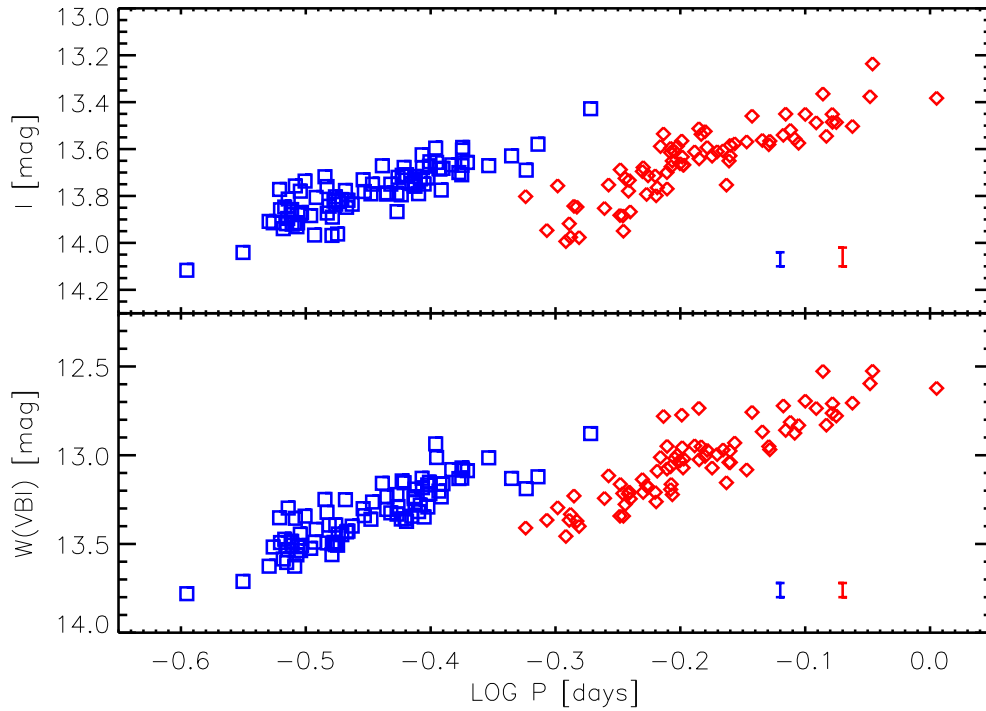
Fig. 12. Top – *I*-band Period-Luminosity relations for fundamental (red) and first overtone (blue) RR Lyrae of the GGC ω Cen (Braga et al. 2016). The vertical bars plotted in the right bottom corner display the standard deviations of the PL relations. Bottom – Triple band (*BVI*) Period-Wesenheit relations for fundamental (red) and first overtone (blue) RR Lyrae in the GGC ω Cen (Braga et al. 2016). The vertical bars plotted in the right bottom corner display the standard deviations of the PW relations.

Indebetouw et al. 2005; Flaherty et al. 2007; Román-Zúñiga et al. 2007) and its variation along different lines of sight (Chapman & Mundy 2009) show that at infrared wavelength the dust extinction is reduced by an order of magnitude when compared with the optical bands. Extinction is at a minimum in the L and M bands where A_V/A_λ ranges from $\simeq 15$ to $\simeq 20$, respectively. At longer wavelengths the extinction increases again due to the occurrence of broad Si-O stretching-mode feature at 9.7 μm and O-Si-O bending mode at 18 μm (Draine 2004). For wavelengths longer than 25 μm the extinction is also reduced, but observations on the Galactic plane are hampered by diffuse thermal emission from filaments in the ISM ("Galactic cirrus").

Based on the reduced extinction, the ideal wavelengths for measuring accurate photometry of CCs and RRLs are the two warm Spitzer/IRAC bands at 3.6 and 4.5 μm. In the case of CCs with period longer than 6 days the 3.6 μm band is preferred, for the presence of variable CO absorption introducing added scatter in their PL relation (Marengo et al. 2010; Scowcroft et al. 2016). The 3.6 μm band is also preferred because of the absence of significant ice features, which are instead observed in the 4.5 μm band (Gibb et al. 2004). Note that the entire L and M wavelength range will also become available as part of the photometric system of the upcoming James Webb Space Telescope.
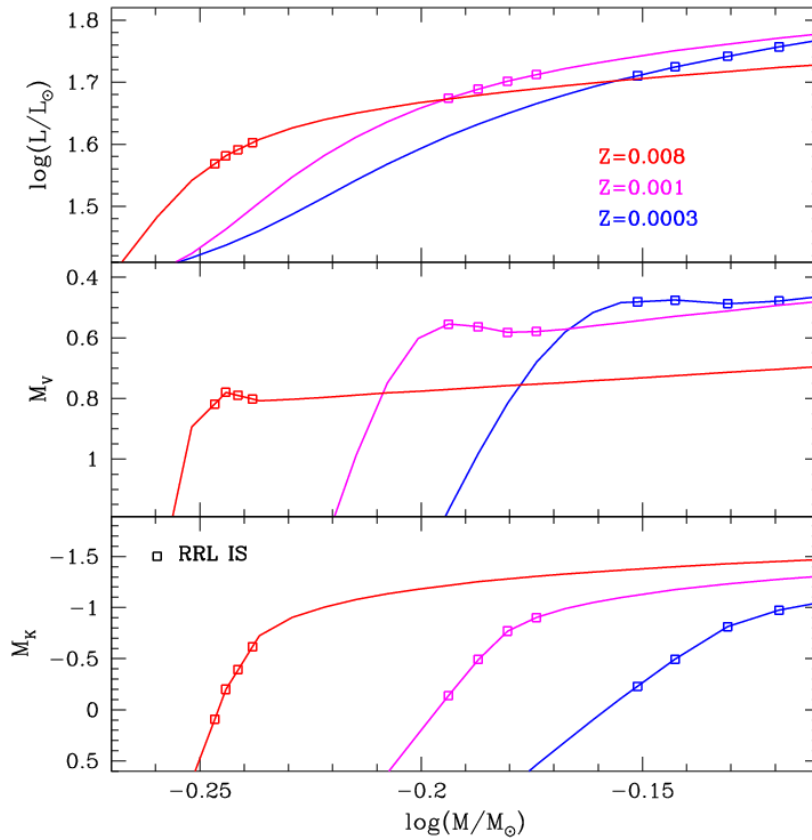
Fig. 13. Top – Predicted Mass-Luminosity relations for low-mass helium burning structures along the ZAHB (Pietrinferni et al. 2006). The blue line shows for metal–poor (Z=0.0003) stellar structures, while the purple for metal–intermediate (Z=0.001) and the red for metal–rich (Z=0.008) stellar structures. The squares mark the location of the instability strip according to Marconi et al. (2015). Middle – Same as the top, but for the visual magnitudes. Bottom – Same as the top, but for the K-band magnitudes. The labels display the period range when moving from the blue to the red edge of the instability strip.

7. Gaia and primary distance indicators

The accuracy and the precision of the cosmic distance scale are going to experience a quantum jump on a very short time. Gaia is going to release the first set of trigonometric parallaxes for the end of 2017 (Gaia collaboration 2016). This means a new spin on all primary distance indicators. Gaia in its early release is delivering distances with an accuracy of the order of 3% or even better, and therefore 6% in distance modulus (Madore et al. 2013). This means that the error budget affecting individual distance estimates based on Period-Luminosity-Metallicity (PLZ) relations $-M_K = \alpha + \beta \log P + \gamma [Fe/H]-$ if we neglect uncertainties on the pulsation period, are dominated by errors in apparent magnitude plus reddening correction and on iron abundance. Note
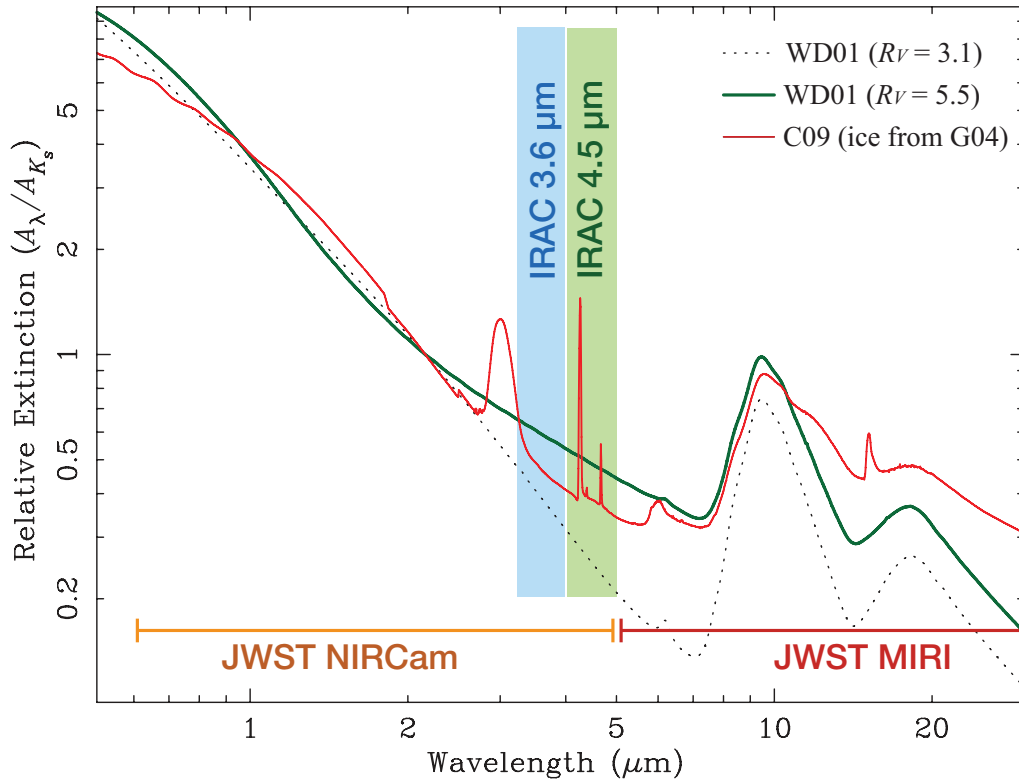
Fig. 14. Interstellar extinction models from Weingartner & Draine (2001) calculated for different values of the selective extinction ratio R_V. The thin red line, according to Chapman & Mundy (2009), includes absorption from interstellar ices identified by Gibb et al. (2004). The figure also shows the bandpasses for the Spitzer/IRAC camera, as well as the wavelength range covered by the James Webb Space Telescope NIRCam and MIRI instruments.

that these uncertainties take account of both intrinsic (photometric error, spectroscopic error) and systematic (absolute calibration, metallicity scale) errors. By assuming the *I*-band PLZ relation for RR Lyrae stars (Marconi et al. 2015), in which the metallicity coefficient is equal to 0.17 mag/dex, and simple statistical arguments, we are left with the evidence that errors on mean magnitudes cannot be larger than 0.03-0.04 mag and the errors on the metal abundance cannot be larger than 0.15-0.20 dex. These are the required accuracies and precisions for both mean magnitudes and metallicities for fully exploiting the precision of Gaia parallaxes. However, the astronomical community is not ready to fully exploit the impact of the new parallaxes. The reason is three-

fold: a) The G magnitudes are the most precise magnitudes delivered by Gaia, but none of the distance diagnostics (PL, PW) is used in this band. Moreover, Gaia metallicities will be based on BP/RP low-resolution spectra approaching a precision of the order of 0.1 dex for G ∼ 15 mag (Liu et al. 2012). b) The closest primary distance indicators (RR Lyrae, classical Cepheids, Miras) do not have accurate optical and NIR mean magnitudes (Neeley et al. 2015). They are too bright for 2-10 m class telescopes and their mean magnitudes are either photographic or not available. c) Metallicity estimates for some of the quoted targets are available, but they are not homogeneous (CCs: Genovali et al. 2014; da Silva et al. 2016; RRLs: Wallerstein & Huang 2010;

For et al. 2011; Pancino et al. 2015). We still lack accurate and homogeneous measurements of iron-peak, s- and r-element abundances. This means that nearby RRLs can be barely used to provide new calibrations of the PLZ and of the Period-Wesenheit-metallicity (PWZ) relations (Braga et al. 2015). Moreover, they cannot constrain the metallicity dependence of the quoted diagnostics, thus hampering the development of new distance scales. These limitations have also a severe impact on the use of RR Lyrae stars as stellar tracers, and in particular, in constraining the metallicity gradient and its spread across the Galactic halo.

8. Spectroscopic surveys

Spectroscopic surveys of CCs and RRLs have been hampered by several technological and intrinsic limits.

a) *Spatial density*– The typical spatial density of CCs across the Galactic thin disk and of RRLs across the Galactic Halo is quite modest (from 1 to a few per square degree). This means that current multi-objects spectrographs can barely be efficient in observing these targets. There are a few exceptions. 1) Cluster variables: this opportunity applies to RRLs (Sollima et al. 2006), since the number of Galactic open clusters hosting sizable samples of CCs is quite modest when compared with the Magellanic Clouds (Pietrzynski & Udalski 1999; Bono et al. 2005). 2) High density regions: the current findings indicate a very high spatial density of RRLs in the inner bulge (Pietrucowicz et al. 2015) and of CCs in the regions located beyond the Galactic center (Matsunaga et al. 2016a). The same outcome applies to the central regions of the Magellanic Clouds.

b) *Intrinsic variability*– CCs and RRLs experience during an entire pulsation cycle a temperature variation ranging from several hundreds (low amplitude variables) to more than one thousand degrees (large amplitude variables), while the surface gravity changes from a few tenths of dex to more than half dex, while the micro-turbulence velocity can change of a few km/sec. The time scale of the variability ranges from a few hours to hundreds of days.

c) *Non-linearities*– RRLs stars during the phases of maximum compression form strong shocks affecting the temperature stratification, and in turn, the optical depth at which both weak and strong lines are formed (Preston 2009, 2011). The problem is less severe for CCs, but they also show evidence of either non-linearity or binarity (Nardetto et al. 2009; Li Causi et al. 2013).

The above evidence have two substantial impacts in devising the observing strategy for radial variables: 1) solid spectroscopic diagnostics need to be adopted to estimate these intrinsic parameters. This means spectra with high spectral resolutions and high signal to noise ratios (SNR). 2) Spectra collected along the pulsation cycle can hardly be co-added to improve the SNR. To overcome these thorny problems we are left with two possible options: i) collect spectra in specific phase intervals; ii) use large telescopes to decrease the exposure time.

Empirical evidence indicates that elemental abundances for both short and long–period Cepheids based on high resolution, high SNR are not affected by the pulsation phase at which they are collected (Luck & Andrievsky 2004; Luck et al. 2008; Romaniello et al. 2008). The RRLs display a more complex behaviour. For et al. (2011) collected roughly 200 spectra for a sample of eleven field RRLs and they showed that iron abundances have, within the errors, minimal changes along the pulsation cycle. They also found clear evidence of NLTE effects in some Si lines between the blue and the red spectral region.

The key spectroscopic advantage in using RRLs and CCs is that their are giants with spectral types range from early F to early K. This means that they are warm and they harbour a large number of lines in the metal-rich and in the metal-poor regime.

The current spectroscopic investigations on CCs (Andrievsky et al. 2002; Yong et al. 2006; Luck et al. 2011; Lemasle et al. 2013; Genovali et al. 2014; Martin et al. 2015) and on RRLs

(For et al. 2011; Pancino et al. 2015) have been performed in the optical to take fully advantage of the high spectral resolution and of the wide wavelength range covered by current echelle spectrographs. The latter properties are mandatory to include a large number of spectroscopic diagnostics required for the estimate of the intrinsic parameters (effective temperature, surface gravity, micro-turbulent velocity) and of elemental abundances.

The lack of a very broad wavelength coverage and the lack of a detailed spectroscopic analysis of the diagnostics that can be used in the NIR regime are the main reasons why the NIR spectroscopic investigations of radial variables is still in its infancy. However, new echelle NIR spectrographs like GIANO (Oliva et al. 2004) and WINERED (Ikeda et al. 2006) are rapidly filling this gap (Fukue et al. 2015). Indeed they provide high spectral resolution, they cover a broad wavelength range and high sensitivity. This means the opportunity to collect high SNR NIR spectra even with 2-4m class telescopes.

These spectrographs also offer the opportunity to be less affected by non-linearities along the pulsation cycle, since the optical regime is mainly dominated by temperature variations, while the NIR regime is dominated by radius variations. This means that NIR spectra collected at random pulsation phases are less and less prone to non-linearities with increasing wavelength respect to optical ones. Note that this is a key advantage for high amplitude short period (HASP) RRLs. These objects are located close to the blue edge of the fundamental RRL instability strip, they are characterized by large pulsation amplitudes (Fiorentino et al. 2015) and develop strong shocks across maximum compression phase (Bono & Stellingwerf 1994). The same outcome applies to mixed-mode (Bono et al. 1996) RRLs and to Blazhko RRLs (Chadid et al. 2011).

On the other hand, NIR spectra do require an optimal subtraction of telluric lines. A significant improvement in this direction comes from very precise modelling of telluric features both in optical and NIR spectra (Seifahrt et al. 2010; Kausch et al. 2015; Smette et al. 2015). To provide a preliminary idea of the impact that the quoted problem has on real spectra Fig. 15 show the optical spectrum of the fundamental RRL V Ind at two different pulsation phases after the subtraction of telluric lines with MOLECFIT (Kausch et al. 2015; Smette et al. 2015). V Ind is a metal-intermediate ([Fe/H]=-1.30, Pancino et al. 2015) field variable for which is available a precise estimate of the individual distance based on the Baade-Wesselink (Clementini et al. 1990). This medium resolution spectrum was collected with X-SHOOTER at VLT. The key advantage of this instrument is that the spectrum simultaneously covers from the UV (λ=2940 Å) to the NIR (λ=23770 Å). Indeed, Fig. 16 shows the NIR portion of the spectrum of the same object collected at the same pulsation phase.

Although the spectral resolution in the NIR regime is quite modest (R~10,000/ 18,000/ 11,000 in the UVB/VIS/NIR arm), several C and α-element (Si, Ti) lines have been clearly identified. This evidence becomes even more compelling if we also take account of the fact that wavelength regime located between the Y- and the J-band also include several diagnostic for constraining the effective temperature (Przybilla et al. 2004; Urbaneja et al. 2005; Przybilla et al. 2009).

9. Future perspectives

The current optical and NIR surveys with ground-base and space facilities provided a new spin on the use of radial variables as stellar tracers. These experiments are complemented by ongoing long-term photometric surveys like OGLE IV. The near future appears even more promising. This applies not only to ground-based optical (iPTF, Rau et al. 2009) and NIR/MIR (TAO, Yoshii et al. 2010) experiments, but also to space experiments (WFIRST, EUCLID). One of the major player in this context is going to be the Large Synoptic Survey Telescope (LSST[1]).

The impact that Gaia is going to have on the cosmic distance scale has already been

---

[1] https://www.lsst.org/
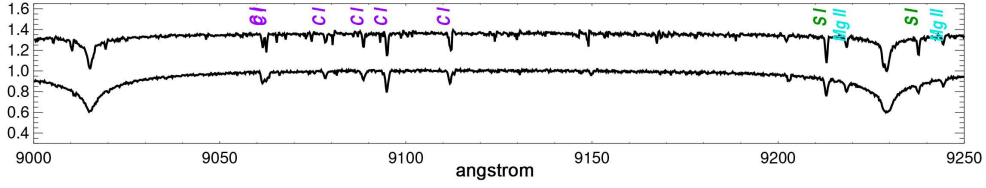
Fig. 15. Optical medium resolution spectrum of the field fundamental RRL V Ind. The spectrum was collected with X-SHOOTER at VLT. Two spectra at different pulsation phases are showed together with the identification of several C and α-element (S, Mg) lines.
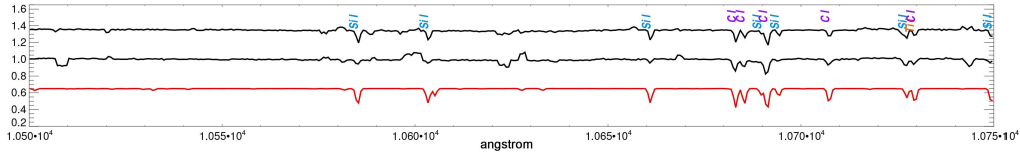
Fig. 16. Same as Fig. 15, but for the NIR region of the spectrum. Note that these spectra were collected simultaneously, since X-Shooter covers from 2940 to 23770 Å. The colored labels on top of the spectrum display the identifications of several C and α-element (Si, Ti) lines.

Table 1. Mass-Luminosity ($\log(\frac{L}{L_\odot})$=a+b*$\log(\frac{M}{M_\odot})$) relations for Classical Cepheids along different crossings of the instability strip. The current predictions are based either on canonical (C) or Non-canonical (N) evolutionary models.

C/N[a]	[M/H]	Y	Z	1st crossing		2nd crossing		3rd crossing		2nd+3rd crossing	
				a	b	a	b	a	b	a	b
C	0.058	0.0198	0.273	0.5817	3.1531	0.6261	3.3782	0.7404	3.3246	0.6871	3.3459
N	0.058	0.0198	0.273	0.6047	3.3827	0.5847	3.6384	0.7707	3.4990	0.6777	3.5687
C	-0.353	0.0080	0.256	0.5665	3.3053	0.8073	3.3355	0.8330	3.3289	0.8201	3.3322
N	-0.353	0.0080	0.256	0.6829	3.4133	0.6899	3.6457	1.1886	3.1085	0.9778	3.3329
C	-0.659	0.0040	0.251	0.5783	3.3953	0.9617	3.2075	0.9502	3.3244	0.9559	3.2659
N	-0.659	0.0040	0.251	0.6980	3.5160	0.9485	3.4368	1.1786	3.2079	1.0635	3.3224
C	-0.963	0.0020	0.248	0.4475	3.7340	1.0000	3.1764	1.2043	3.0465	1.1022	3.1892
N	-0.963	0.0020	0.248	0.9113	3.2899	1.2026	3.2113	1.2674	3.1670	1.2350	3.1114

Table 2. Predicted stellar luminosity, effective temperature and period for fundamental RRLs with different metal abundances (Z) at the edges of the instability strip (Marconi et al. 2015).

Z	$\frac{M}{M_\odot}$	$\log \frac{L}{L_\odot}$	$\log T_e$	P [days]
0.0003	0.7061	1.710283	3.859200	0.3836
0.0003	0.7600	1.756874	3.773928	0.7905
0.0010	0.6400	1.674198	3.859540	0.3881
0.0010	0.6700	1.712249	3.769130	0.8323
0.0080	0.5667	1.568359	3.856920	0.3625
0.0080	0.5779	1.602434	3.773430	0.7436

discussed in detail in the recent literature (Thévenin 2008; Eyer et al. 2012). Here we only mention that Gaia's absolute calibrations of primary distance indicators will be a fundamental stepping stone to investigate the 3D structure of nearby stellar systems (de Grijs & Bono 2014, 2015).

A cursory look to the astrophysical and cosmological impact of LSST (Ivezić 2010) reveals an outstanding range of implications from the minor bodies of the Solar System to the nature of dark energy and dark matter. However, the scientific framework becomes even more clear if we take account for the fact that LSST is going to survey the entire Southern sky in six different photometric bands (*ugrizy*) with limiting magnitudes for individual frames ranging from 22 (*y*) to 25 (*g*) and co-added final magnitudes ranging from 25 (*y*) to 27.5 (*r*) mag. The observing strategy was designed to cover the entire Southern sky every three days (the field of view is roughly 10 square degrees) and the total number of visits per pointing, over the ten years of the project, ranges from roughly 50 (*u*) to more than 180 (*r,i*). The above numbers indicate that LSST, when compared with Gaia, is going to be at least five magnitudes fainter and covering the entire range of spectral types. LSST will provide the unique opportunity to recover the time axis in a broad range of astrophysical phenomena, together with a very good image quality (pixel scale 0.2 arcsec/px) and accuracy in photometric and astrometric measurements of point-like objects. This means that LSST is going to be a quantum jump for transients and in particular for stellar variability.

The selection of the diagnostic to perform accurate and precise abundance analysis of NIR spectra is paving the way to the science objectives we plan to accomplish with Extremely Large Telescopes (ELTs). The first light instruments for the European-ELT[2]

(MICADO/MAORY[3]; HARMONI[4]; METIS[5]) include either a medium or a high spectral resolution NIR/MIR spectrograph. Note that the difference in spectral resolution between HARMONI and NIRSPEC at the James Webb Space Telescope (JWST[6]) is almost one order of magnitude (R$\sim$ 20,000 [0.9–2.2 μm] vs 1000–2700 [1–5 μm]). The difference becomes even larger in the MIR regime, and indeed METIS is planning to observe at 3.78–4.66 μm with a spectral resolution $\sim$100,000.

The above difference becomes even more compelling if account for the fact that the pixel scale for MICADO/MAORY (0.003 arcsec/px) is at least a factor of ten smaller than the current pixel scale of the Advanced Camera for Surveys (0.027 arcsec/px) at the Hubble Space Telescope[7] and of the pixel scale for NIRCAM[8] (0.03 arcsec/px) at JWST. This means that ELTs and the new adaptive optics systems are going to play a crucial role to perform accurate NIR photometry in crowded and reddened regions of the Galactic bulge/center/plane and of nearby galaxies.

On the other hand, both NIRCAM and NIRSPEC have FoVs that are significantly larger than the first light instruments at E-ELT. The synergy among near future ground-based and space observing facilities becomes even more interesting if we also account for the first generation of E-ELT instruments, namely the high-resolution optical/NIR spectrograph HIRES[9] (Maiolino et al. 2013) and for the low/medium resolution optical/NIR multi-object spectrograph MOSAIC[10] (Evans et al. 2014).

---

[2] https://www.eso.org/sci/facilities/eelt/

[3] https://www.eso.org/public/italy/teles-instr/e-elt/e-elt-instr/micado/ ; https://www.eso.org/public/italy/teles-instr/e-elt/e-elt-instr/maory/ ; http://www.mpe.mpg.de/ir/micado

[4] https://www.eso.org/public/italy/teles-instr/e-elt/e-elt-instr/harmoni/

[5] https://www.eso.org/public/italy/teles-instr/e-elt/e-elt-instr/metis/ ; http://metis.strw.leidenuniv.nl/

[6] http://jwst.nasa.gov/instruments.html

[7] http://hubblesite.org/

[8] http://www.stsci.edu/jwst/instruments/nircam

[9] http://www.hires-eelt.org/

[10] http://mosaic.obspm.fr/

References

Alcock, C., et al. 2000, ApJ, 542, 281

Anderson, R. I., et al. 2014, A&A, 564, A100

Anderson, R.I., et al. 2016, A&A, 591, 8

Andrievsky, S. M., et al. 2002, A&A, 381, 32

Asplund, M. et al. 2009, A&A Rev., 47, 481

Barnes, T.G., et al. 1988, ApJS, 67, 403

Beaton, R. L., Freedman, W. L., Madore, B. F., et al. 2016, arXiv:1604.01788

Bohm-Vitense, E. 1988, ApJ, 324, L27

Bono, G., & Stellingwerf, R. F. 1994, ApJS, 93, 233

Bono, G., et al. 1996, ApJ, 471, L33

Bono, G., et al. 1997, A&AS, 121, 327

Bono, G., et al. 1997, ApJ, 477, 346

Bono, G., Marconi, M., & Stellingwerf, R. F. 2000, A&A, 360, 245

Bono, G., Caputo, F., & Marconi, M. 2001, MNRAS, 325, 1353

Bono, G., et al. 2003, MNRAS, 344, 1097

Bono, G., et al. 2005, ApJ, 621, 966

Bono, G., et al. 2010, ApJ, 715, 277

Braga, V.F., et al. 2015, ApJ, 799, 165

Braga, V.F., et al. 2016, arXiv:1609.04916

Brocato, E., & Castellani, V. 1993, ApJ, 410, 99

Bryant, P.H. 2014, ApJ, 783, 15

Buchler, J. R. 2009, American Institute of Physics Conference Series, 1170, 51

Cacciari, C., et al. 1987, A&AS, 69, 135

Calamida, A., et al. 2005, ApJ, 634, L69

Caputo, F. 1998, A&A Rev., 9, 33

Caputo, F., et al. 2000, MNRAS, 316, 819

Cardelli, J. A., Clayton, G. C., & Mathis, J. S. 1989, ApJ, 345, 245

Cassisi, S., & Salaris, M. 2011, ApJ, 728, L43

Castellani, V., Chieffi, A., & Straniero, O. 1990, ApJS, 74, 463

Castellani, V., et al. 2007, ApJ, 663, 1021

Chadid, M., et al. 2011, A&A, 527A, 146

Chapman, N. L., & Mundy, L. G. 2009, ApJ, 699, 1866

Chiosi, C., & Maeder, A. 1986, ARA&A, 24, 329

Cioni, M.-R. L. et al. 2011, A&A, 527, A116

Clement, C. M., & Rowe, J. 2000, AJ, 120, 2579

Clementini, G., et al. 1990, A&AS, 85, 865

Coppola, G., et al. 2015, ApJ, 814, 71

Cox, A. N. 1980, ARA&A, 18, 15

Cutri, R. M., & et al. 2013, VizieR Online Data Catalog, 2328

Dall'Ora, M., et al. 2003, AJ, 126, 197

Dalton, G., et al. 2014, Proc. SPIE, 9147, 91470L

da Silva, R., et al. 2016, A&A, 586, A125

de Grijs, R., & Bono, G. 2014, AJ, 148, 17

de Grijs, R., & Bono, G. 2015, AJ, 149, 179

de Jong, R. S., et al. 2014, Proc. SPIE, 9147, 91470M

Draine, B. T. 2004, in Origin and Evolution of the Elements, ed. A. McWilliam and M. Rauch (Cambridge Univ. Press, Cambridge), 317

Drake, A.J., et al. 2014, ApJS, 213, 9

Evans, C. J., et al. 2014, Proc. SPIE, 9147, 914796

Eyer, L., et al. 2012, Ap&SS, 341, 207

Faber, S.M., et al. 2003, Proc. SPIE, 4841, 1657

Fiorentino, G., et al. 2015, ApJ, 798, 12

Flaherty, K. M., et al. 2007, ApJ, 663, 1069

For, B.-Q., Sneden, C., & Preston, G. W. 2011, ApJS, 197, 29

Freedman, W. L., Madore, B. F., Scowcroft, V., et al. 2012, ApJ, 758, 24

Fukue, K., et al. 2015, ApJ, 812, 64

Gaia collaboration 2016, A&A, in press

Genovali, K., et al.2014, A&A, 566A, 37

Gibb, E. L., et al. 2004, ApJS, 151, 35

Grevesse, N., & Noels, A. 1993, in Origin and Evolution of the Elements, ed. A. McWilliam and M. Rauch (Cambridge Univ. Press, Cambridge), 15

Gunn, J.E., et al. 1998, AJ, 116, 3040

Hendricks, B., et al. 2012, AJ, 144, 25

Hook, I. M., et al. 2004, PASP, 116, 425

Ikeda, Y., et al. 2006, Proc. SPIE, 6269, 62693T

Indebetouw, R., et al. 2005, ApJ, 619, 931

Inno, L., et al. 2015, A&A, 576, A30

Inno, L., et al. 2016, ApJ, arXiv:1609.03554

Ivezić, Ž. 2010, Highlights of Astronomy, 15, 188

Jones, R.V., et al. 1992, ApJ, 386, 646

Kausch, W., et al. 2015, A&A, 576, A78

Kunder, A., et al. 2012, AJ, 143, 57

Kunder, A., et al. 2013, AJ, 146, 119

Laney, C. D., & Stobie, R. S. 1992, A&AS, 93, 93

Lemasle, B., et al. 2013, A&A, 558, A31

Le Fèvre, O., et al. 2003, Proc. SPIE, 4841, 1670

Li Causi, G., et al. 2013, A&A, 549, A64

Liu, T. & Janes, K.A. 1989, ApJS, 69, 593

Liu, C., et al. 2012, MNRAS, 426, 2463

Longmore, A. J., Fernley, J. A., & Jameson, R. F. 1986, MNRAS, 220, 279

Luck, R. E., & Andrievsky, S. M. 2004, AJ, 128, 343

Luck, R. E., et al. 2008, AJ, 136, 98

Luck, R. E., & Lambert, D. L. 2011, AJ, 142, 136

Madore, B. F. 1982 ApJ, 253, 575

Madore, B. F., et al. 2013, ApJ, 776, 135

Maiolino, R., et al. 2013, arXiv:1310.31635

Majewski, S. R., et al. 2015, arXiv:1509.05420

Malavolta, L., et al. 2014, AJ, 147, 25

Marconi, M., et al. 2015, ApJ, 808, 50

Marengo, M., et al. 2010, ApJ, 709, 120

Marquette, J.B., et al. 2009, A&A, 495, 249

Martin, R. P., et al. 2015, MNRAS, 449, 4071

Martínez-Vázquez, C. E., et al. 2015, MNRAS, 454, 1509

Mateo, M., et al. 2012, Proc. SPIE, 8446, 84464Y

Matsunaga, N., et al. 2016, MNRAS, 462, 414

Matsunaga, N., et al. 2017, in Astronomical Distance Determination in the Space Age, (Springer), Space Science Series of ISSI-BJ, in preparation

McConnachie, A. W., et al. 2016, arXiv:1606.00060

McLean, I. S., et al. 2012, Proc. SPIE, 8446, 84460J

McWilliam, A. 2016, PASA, 33, e040

Minniti, D., et al. 2010, New Astron., 15, 433

Molnar, L. 2016, Comm. Konkoly Obs., 105, 14

Moskalik, P., Buchler, J. R., & Marom, A. 1992, ApJ, 385, 685

Nardetto, N., et al. 2008, A&A, 489, 1255

Nardetto, N., et al. 2009, A&A, 502, 951

Neeley, J. R., et al. 2015, ApJ, 808, 11

Ness, M., et al. 2012, ApJ, 756, 22

Ngeow, C.-C., & Kanbur, S. M. 2010, ApJ, 720, 626

Oliva, E., et al. 2004, Proc. SPIE, 5492, 1274

Pancino, E., et al. 2015, MNRAS, 447, 2404

Pasquini, L., et al. 2002, The Messenger, 110, 1

Persson, S. E., et al. 2004, AJ, 128, 2239

Pietrinferni, A., et al. 2004, ApJ, 612, 168

Pietrinferni, A., et al. 2006, ApJ, 642, 797

Pietrukowicz, P., et al. 2015, ApJ, 811, 113

Pietrzynski, G., & Udalski, A. 1999, Acta Astron., 49, 543

Pojmansi, G., Pilecki, B. & Szczygiel, D. 2005, Acta Astron., 55, 275

Poretti, E., et al. 2010, A&A, 520A, 108

Poretti, E., Baglin, A., & Weiss, W. W. 2014, ApJ, 795, L36

Prada-Moroni, P.G., et al. 2012, ApJ, 749, 108

Preston, G. W. 2009, A&A, 507, 1621

Preston, G. W. 2011, AJ, 141, 6

Proxauf, B., et al. 2016, Master Thesis, University of Rome Tor Vergata

Przybilla, N., Butler, K., Becker, S. R., Kudritzki, R. P. 2004, in Origin and Evolution of the Elements, ed. A. McWilliam and M. Rauch (Carnegie Obs., Pasadena), Carnagie Obs. Astroph. Ser., 4, 48

Przybilla, N., et al. 2009, ASSP, 9, 55

Rau, A., et al. 2009, PASP, 121, 1334

Rey, S.-C., et al. 2000, AJ, 119, 1824

Rieke, G. H., & Lebofsky, M. J. 1985, ApJ, 288, 618

Riess, A. G., et al. 2016, ApJ, 826, 56

Román-Zúñiga, C. G., et al. 2007, ApJ, 664, 357

Romaniello, M., et al. 2008, A&A, 488, 731

Sandage, A. 1990, ApJ, 350, 603

Scowcroft, V., et al. 2016, MNRAS, 459, 1170

Seifahrt, A., et al. 2010, A&A, 524, A11

Sollima, A., et al. 2006, ApJ, 640, L43

Sasselov, D. D., & Lester, J. B. 1994, ApJ, 423, 795

Smette, A., et al. 2015, A&A, 576, A77

Soszynski, I., et al. 2014, Acta Astron., 64, 177

Soszyński, I., Udalski, A., Szymański, M. K., et al. 2015, Acta Astron., 65, 297

Steinmetz, M., et al. 2006, AJ, 132, 1645

Stetson, P.B., et al. 2014, PASP, 126, 521

Stothers, R. B. 2006, ApJ, 652, 643

Stothers, R. B., & Chin, C.-W. 1993, ApJ, 412, 294

Stothers, R. B., & Chin, C.-W. 1994, ApJ, 431, 797

Thévenin, F. 2008, Physica Scripta Volume T, 133, 014010

Torrealba, G., et al. 2015, MNRAS, 446, 2251

Udalski, A., et al. 1993, Acta Astron., 43, 69

Udalski, A., et al. 1998, Acta Astron. 48, 1

Udalski, A., Szymanski, M.K & Szymanski, G. 2015, Acta Astron., 65, 1

Urbaneja, M. A., et al. 2005, ApJ, 622, 862

Wallerstein, G., & Huang, W. 2010, MmSAI, 81, 952

Weingartner, J. C., & Draine, B. T. 2001, ApJS, 134, 263

Welch, D. L., et al. 1987, ApJ, 321, 162

Yong, D., et al. 2006, AJ, 131, 2256

Yoshii, Y., et al. 2010, Proc. SPIE, 7733, 773308

Zoccali, M., et al. 2004, A&A, 423, 507

[1] Dipartimento di Fisica, Università di Roma Tor Vergata, Via della Ricerca Scientifica 1, 00133 Roma, Italy
e-mail: bono@roma2.infn.it

[2] INAF-OAR, via Frascati 33, 00040 Monte Porzio Catone, Italy

[3] ASDC, via del Politecnico snc, 00133 Roma, Italy

[4] INAF-OATe, Via Mentore Maggini snc, Loc. Collurania, 64100 Teramo, Italy

[5] INAF-OAC, Salita Moiariello 16, 80131 Napoli, Italy

[6] INAF-OABo, Via Ranzani 1, 40127 Bologna, Italy

[7] Institute of Astronomy, Univ. of Tokyo, 2-21-1 Osawa, Mitaka, Tokyo 181-0015, Japan

[8] MPIA Heidelberg, Königstuhl 17, 69117 Heidelberg, Germany

[9] Department of Physics and Astronomy, Iowa State University, Ames, IA 50011, USA

[10] ESO, Karl-Schwarzschild-Str. 2, 85748 Garching bei Munchen, Germany

[11] Univ. of Vienna, Department of Astrophysics, Türkenschanzstr. 17, 1180 Vienna, Austria

[12] Inst. Astro Teilchenphysik, Univ. Innsbruck, Techniker 25/8, 6020 Innsbruck, Austria

[13] Odessa National University, Shevchenko Park, 65014, Odessa, Ukraine

[14] Astron. Rechen-Institut, Univ. Heidelberg, Mönchhof 12, D-69120 Heidelberg, Germany

[15] IAC, Calle Via Lactea s/n, E38205 La Laguna, Tenerife, Spain

[16] INAF-OATs, Via G.B. Tiepolo, 11, 34143 Trieste, Italy

[17] MPS Göttingen, Justus-von-Liebig-Weg 3, 37077 Göttingen, Germany

[18] John Moores Univ., Liverpool Science Park, 146 Brownlow Hill, Liverpool, L3 5RF, UK

[19] Dept. of Astronomy C1400, University of Texas, Austin, TX 78712, USA

[20] NRC-Herzberg, DAO, 5071 West Saanich Road, Victoria BC V9E 2E7, Canada

[21] Univ. Côte d'Azur, Obs. de Nice, Lab. Lagrange CNRS, CS 34229, 06304 Nice, France

[22] NAOJ, 2-21-1 Osawa, Mitaka, Tokyo 181-8588, Japan

[23] Pontificia Universidad Catolica de Chile, Av. B. O'Higgins 328, Santiago, Chile

[24] Millennium Institute of Astrophysics, Av. Vicuña Mackenna 4860, Santiago, Chile